Hotspot-Induced Transformation of Surface-Enhanced Raman Scattering Fingerprints

Tao Chen,[†] Hong Wang,[†] Gang Chen,[†] Yong Wang,[†] Yuhua Feng,[†] Wei Shan Teo,[†] Tom Wu,[‡] and Hongyu Chen[†,*]

[†]Division of Chemistry and Biological Chemistry and [‡]Division of Physics and Applied Physics, School of Physical and Mathematic Sciences, Nanyang Technological University, 21 Nanyang Link, Singapore 637371

ABSTRACT The most studied effect of surface-enhanced Raman scattering (SERS) hotspots is the enormous Raman enhancement of the analytes therein. A less known effect, though, is that the formation of hotspots may cause the trapped analytes to change molecular orientation, which in turn leads to pronounced changes in SERS fingerprints. Here, we demonstrate this effect by creating and characterizing hotspots in colloidal solutions. Anisotropically functionalized Au nanorods were synthesized, whereby the sides were specifically encapsulated by polystyrene-*block*-poly(acrylic acid), leaving the ends unencapsulated and functionalized by a SERS analyte, 4-mercaptobenzoic acid. Upon salt treatment, these nanorods assemble into linear chains, forming hotspots that incorporate the SERS analyte. Enormous SERS enhancement was observed, particularly for some weak/inactive SERS modes that were not present in the original spectrum before the hotspots formation. Detailed spectral analysis showed that the variations of the SERS fingerprint were consistent with the reorientation of analyte molecules from nearly upright to parallel/tilted conformation on the Au surface. We propose that the aggregation of Au nanorods exerts physical stress on the analytes in the hotspots, causing the molecular reorientation. Such a hotspot-induced variation of SERS fingerprints was also observed in several other systems using different analytes.

KEYWORDS: SERS · fingerprint · hotspot · Au nanorod · linear aggregation

Surface-enhanced Raman scattering (SERS) is an alternative to fluorescence for ultrasensitive optical detection.[1−3] It greatly amplifies the Raman signal of analytes adsorbed on a metal surface, particularly at "hotspots" such as junctions or gaps between metal nanoparticles.[4,5] The most studied effect of SERS hotspots is the enhanced local electric field which gives rise to the enormous SERS enhancement; other effects, such as the alteration of SERS fingerprints as reported here, have not been fully explored.

SERS fingerprints provide highly specific characterization of the respective analytes. Combined with the gigantic enhancement at hotspots, this would lead to powerful platforms for multiplexed sensing and detection.[6] Hence, it is critical to explore the variability of SERS fingerprints and especially the unique influence exerted by a hotspot. The peaks of a SERS spectrum originate from the various vibrational modes of an analyte. It is generally accepted from theoretical perspectives that the molecular orientation on a metal surface would affect both the electromagnetic enhancement, which is strongest when a vibrational mode aligns with local electric field (surface selection rule),[7,8] and the chemical enhancement, which is sensitive to the orbital couplings in a metal−analyte complex.[9] While it is conceivable that hotspots may exert physical stress on the trapped analytes, causing alterations in molecular orientation, few reports documented the variations of SERS response as a result of hotspot formation. Indeed, only a handful of reports studied the dependence of SERS response on other experimental conditions[10−14] such as the concentration of an analyte during its adsorption, which was often interpreted as affecting the molecular density and thus the orientation.[12] The challenges in studying hotspot-induced SERS variation are inherent in the characterization methods, which are so far mostly based on single-molecule or single-nanocluster techniques.[15,16] The photodamage of analytes[17] and the blinking of single-molecule SERS,[3,16] in particular, add to the ambiguities in assigning the origin of spectral changes.

Notably, the inadequate capability in fabricating uniform and consistent SERS hotspots has limited the development of both single-molecule and ensemble studies. So far, most of the studies generated hotspots by salt-induced aggregation or chemical linking of metal nanoparticles,[3,18−20] which inevitably led to a mixture of nanoclusters of various sizes and structures. While this nonuniformity

*Address correspondence to hongyuchen@ntu.edu.sg.

Received for review February 9, 2010 and accepted May 24, 2010.

Published online May 28, 2010. 10.1021/nn100269v

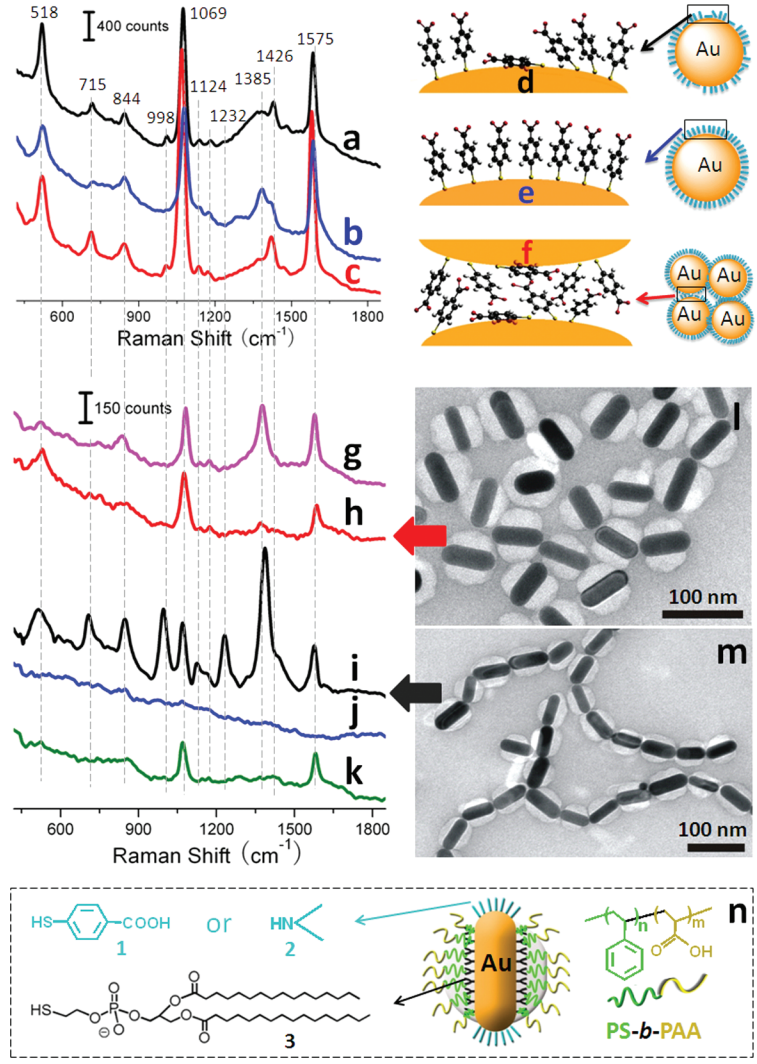

Figure 1. SERS spectra of (a) AuNSs incubated with 1 at room temperature; (b) sample a after further incubation at 60 °C for 3 h; and (c) sample b after the aggregation induced by 0.044 M NaCl and 2.95 M NaOH. (d−f) Schematic illustrations of the surface ligands corresponding to a−c. The scheme was for illustration purposes; in reality, the ligands could form denser packing than illustrated and those in e could be slightly tilted owing to intermolecular van der Waals interactions. (g) Raman spectrum of 50 mM 1 in 5 M aq NaOH; (h) SERS spectrum of *aniso*-(1+3-AuNR)@PSPAA; (i) SERS spectrum of sample h after the salt-induced linear aggregation and the purification to remove the salts (the aggregates were redispersed in the same volume of water); (j) absence of SERS in linearly aggregated *aniso*-(2+3-AuNR)@PSPAA; (k) SERS spectrum of sample j after incubation with 1 at 60 °C for 24 h; (l and m) TEM images of *aniso*-(1+3-AuNR)@PSPAA and their linear aggregates; and (n) schematics showing the structure of *aniso*-AuNR@PSPAA. Spectra are offset for clarity.

among the individual nanoclusters is not a major issue for single-nanocluster studies, it poses additional challenges in interpreting the origin of any spectral variations, even if observed. Most recently, significant advances have been made in fabricating more uniform nanostructures,[17,21−26] and this provides new opportunities for characterizing the chemical and physical effects within the unique environment of hotspots.

Herein, hotspot-induced transformation of SERS response was characterized and analyzed. The specific encapsulation of the sides but not the ends of Au nanorods (NRs) allowed us to construct consistent hotspots by linear aggregation (Figure 1m).[27] This structural feature helped to localize the analytes and to pinpoint the location of SERS response in the event of hotspot formation. A dramatic change in the SERS fingerprint was observed when 4-mercaptobenzoic acid (**1**) was trapped in the hotspots (Figure 1i *vs* 1h). On the basis of detailed spectral analysis, we proposed that this phenomenon was due to the orientation change of **1**, possibly induced by the physical stress associated with hotspot formation. Such hotspot-induced effect could be quite general as it was observed for several other analytes.

We focused our study on colloidal systems;[28,29] all Raman spectra reported here were collected from sample solutions in quartz cuvetts using 785 nm LED laser at 290 mW, typically averaged over 30 s for each spectrum. Thus, the SERS responses from a collection of nanoparticles were studied, and this approach averages out the inhomogeneity in the SERS of analyte molecules. Most importantly, the dynamic diffusion of nano-

clusters in and out of the laser focal point during SERS measurements minimizes the exposure of any particular nanocluster, and the photothermal energy at the hotspots could be quickly dissipated to the surrounding media. These features minimize the photodamage of analytes, particularly for those in the hotspots under a very high electromagnetic field. In fact, in all of our colloidal SERS measurements, we did not observe any spectral changes as a result of prolonged laser irradiation.

RESULTS AND DISCUSSION

It was initially noticed that when **1**-coated Au nanospheres (**1**-AuNSs) were aggregated, the SERS peaks were not enhanced equally by the hotspot formation (Figure 1b,c), with prominent changes occurring at 715, 998, and 1124 cm^{-1}. Since these peaks were often absent or very weak in the SERS of **1**,[30−32] it appears that there were other effects at work, in addition to the local field enhancement at hotspots. Detailed study showed that the peaks already existed, though in low intensity, when **1** was simply incubated with 98 nm AuNSs at room temperature (Figure 1a), but they mostly disappeared after incubation at 60 °C for 3 h (Figure 1b). The large size of AuNSs used here helped in revealing the low-intensity peaks.

Previously, **1** and similar compounds were studied in detail on bulk Au substrates.[30−33] The SERS of **1** typically includes the ring breathing modes at 1069 and 1575 cm^{-1} and the COO^- stretching mode at 1385 cm^{-1},[30−32] which are characteristic of **1** bonded on a Au surface through the thiol group in a nearly upright conformation.[30] The 715 cm^{-1} peak was assigned to an out-of-plane CCC-bending mode, which does not align with the surface normal (i.e., the direction of local electric field) if **1** is in an upright conformation. On the basis of the surface selection rule, the appearance of this peak is an indication for tilted/parallel conformation of **1**.[31] The peaks at 998 and 1124 cm^{-1} may be enhanced by strong surface−π conjugation; they are almost identical to the in-plane vibrations of the phenyl ring in the SERS of 1,4-benzenedithiol,[34,35] which was known to attach parallel on a metal surface *via* both thiol groups. It has been previously suggested that the parallel conformation facilitated the surface−π conjugation, which strongly enhanced the two peaks.[35] Therefore, the presence of the three peaks at 715, 998, and 1124 cm^{-1} in Figure 1a suggested that some molecules of **1** were in tilted/parallel conformation. A small percentage of such defects are expected for **1**-AuNSs prepared at room temperature (Figure 1d). After the incubation at 60 °C, the three peaks reduced in intensity (Figure 1b), indicating the removal of most of the defect sites and the packing of **1** in predominantly upright conformation (Figure 1e).[36]

The **1**-AuNSs in samples 1a and 1b (of Figure 1a and 1b) were not aggregated based on the single absorption peak at 550 nm in UV−vis−NIR absorption spectra (see Supporting Information); upon NaCl addition the increased absorbance at longer wavelength (800−1000 nm) suggested significant aggregation of the **1**-AuNSs. After the aggregation, the three SERS peaks at 715, 998, and 1124 cm^{-1} reappeared (Figure 1c); compared to the other peaks in Figure 1b, the enhancement of the three peaks was slightly more pronounced. However, the spectral difference between Figure 1b and 1c was too small to provide mechanistic insights. Although one could argue that the specific enhancement of the three peaks could be attributed to the formation of tilted **1** (Figure 1f), it is also possible that the enhancement of a small number of remaining tilted **1** by hotspots could be solely responsible. Furthermore, in the random aggregates there exist a variety of SERS hotspots with different structures. It is difficult to attribute the spectral changes to a specific structural feature. Therefore, we adapted a new nanofabrication method to further explore this phenomenon.

Recently, we reported the anisotropic encapsulation of AuNRs by polystyrene-*block*-poly(acrylic acid) (PSPAA).[27] This was realized by virtue of competitive ligand adsorption,[27,37] in which the hydrophobic ligand (such as 2-dipalmitoyl-*sn*-glycero-3-phosphothioethanol, **3**, Figure 1n) ended up on the sides of the AuNRs and embedded in the polymer shell, whereas the hydrophilic ligand (such as **1**) localized on the ends and was exposed to the solution (Figure 1l and 1n, denoted as *aniso*-(**1**+**3**-AuNR)@PSPAA). Here, **1** is SERS-active while **3** is virtually SERS-inactive. The SERS spectrum (Figure 1h) is consistent with SERS of **1** in a nearly upright conformation[30,31] and is also similar to the ordinary Raman scattering of **1** in aq NaOH (Figure 1g).

The *aniso*-(**1**+**3**-AuNR)@PSPAA particles were induced to aggregate in concentrated NaCl and NaOH, and then they were purified in water to remove the salt. As the PSPAA micelles are resistant to aggregation under such conditions,[24] the unique core/shell structure of *aniso*-(**1**+**3**-AuNR)@PSPAA dictated the linear arrangement of the AuNRs (Figure 1m). The additional absorption peak centered at 888 nm after the aggregation (Figure 2b) is significantly red-shifted from the longitudinal plasmon peak of nonaggregated AuNRs (673 nm, Figure 2a). It could be attributed to the plasmon coupling along the linear chains. Thus, both the TEM image and particularly the UV−vis−NIR absorption spectra support the formation of linear chains in solution.

After the aggregation, SERS analyte **1** is localized at the area that made up the hotspots, highlighting the distinctive spectral response therein. The SERS spectrum underwent dramatic transformation (Figure 1i) compared to that of the nonaggregated sample (Figure 1h). Since the spectrum did not vary as a function of time, the aggregation-induced spectral change was likely not caused by inhomogeneity in the SERS re-

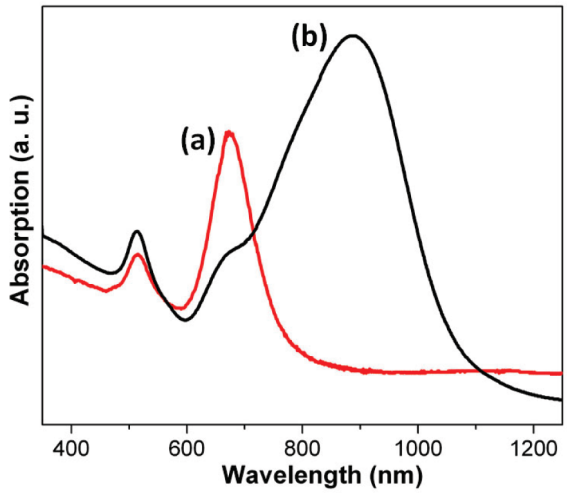

Figure 2. UV−vis−NIR absorption spectra of (a) *aniso*-(1+3-AuNR)@PSPAA, and (b) sample a after salt-induced aggregation and the subsequent purification, *i.e.*, linear chains of *aniso*-(1+3-AuNR)@PSPAA.

sponse from molecules in hotspots. All peaks increased in intensity except the 1069 cm^{-1} peak, and the most pronounced changes occurred at 715, 998, and 1124 cm^{-1}, where the peaks were initially barely observable.[30−32] As discussed above, the presence of the three peaks is an indication for the formation of tilted/parallel **1** on Au surfaces, which may arise from the physical stress in the hotspots. This argument is reasonable considering that the AuNRs were probably under similar forces in forming the linear aggregates. Unlike the case discussed above, however, the much stronger enhancement of the three peaks here cannot be solely explained by the field enhancement at hotspots. In addition, there was probably a significant increase in the percentage of tilted **1** in the hotspots. The combination of both effects gave rise to the exceptional enhancement. In contrast, although the SERS of upright **1** was also greatly enhanced by the hotspots, the decrease in the number of such molecules counteracted and led to weaker peak intensities. Had the number of upright **1** remained unchanged, the ring breathing modes (1069 and 1575 cm^{-1}) aligning with the local electric field would have been greatly enhanced by the hotspots.

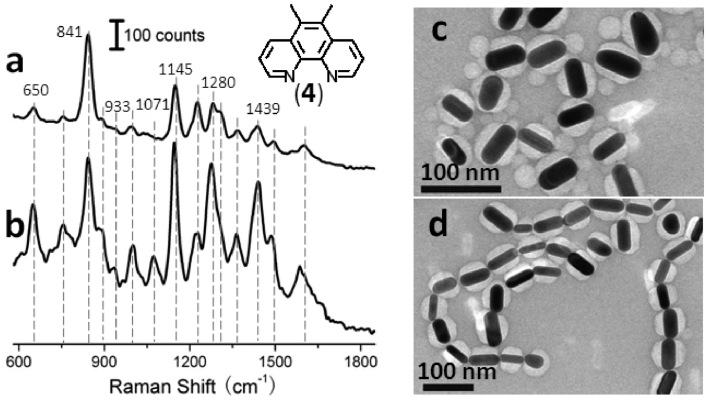

Figure 3. SERS spectra of (a) *aniso*-(2+3-AuNR)@PSPAA after incubation with 4; and (b) sample a after salt-induced aggregation, *i.e.*, linear chains of *aniso*-(4+3-AuNR)@PSPAA; (c and d) TEM images of the samples a and b.

It should be noted that the packing of **1** on the Au surface could possibly make the surface molecules slightly tilted relative to the surface normal, in order to maximize the van der Waals interactions among them. The tilting of a long alkanethiol in a self-assembled monolayer on a Au surface was known to be pronounced.[36] But in our system, since Figure 1b showed only very weak peaks that could be attributed to tilted **1**, it is unlikely that the slight tilting of **1** could contribute significantly to the SERS spectra.

On the other hand, the local field intensity between the AuNRs should be strongest at the contact point, where the gap distance is the shortest.[5,18] The lengthening of the AuNRs along the longitudinal direction further enhanced the coupling between the AuNRs and thus the field intensity at the contact points.[5,18,38] Hence, the tilted molecules at hotspots were favorably enhanced, and this explains the dramatic spectral changes (Figure 1h,i) in this particular system. The molecular reorientation from nearly upright to tilted/parallel conformation probably only occurred in the very small area at the contact point between the ends of neighboring AuNRs, as opposed to, for example, inside a trigonal cavity of a random aggregate of NSs. The rest of the SERS peaks are also consistent with our explanation. The enhancement of COO^- vibrational modes[31] at 844 and 1385 cm^{-1} could be partially attributed to the local field enhancement at hotspots.[5] Moreover, the proximity of carboxylic groups to the Au surface (*e.g.*, of neighboring AuNR, Figure 1f) may lead to chemical enhancement *via* bond formation.[39] The 1232 cm^{-1} peak, being a C−O stretching mode,[40] was probably enhanced by a similar mechanism.

In randomly aggregated **1**-AuNSs, the SERS response from hotspots was not favorably enhanced. SERS enhancement generally increases with the size of nanoparticle/nanocluster. But random aggregation of the **1**-AuNSs could not create large structures without enclosing the resulting hotspots. The hotspots *inside* the nanoclusters should not contribute much to the overall SERS spectrum, as both the incident radiation and the SERS response could be attenuated by the absorption and scattering of the neighboring AuNSs. In addition, the analyte **1** coats the entire surface of the nanoclusters, including the inner surface of the cavities. On large nanoclusters, the SERS contribution from the unstressed surface analytes could be quite significant. This is in contrast to the *aniso*-AuNR@PSPAA that formed extensive plasmon coupling in only one dimension. Thus, it is understandable that the changes of SERS fingerprint for the randomly aggregated **1**-AuNSs (Figure 1c) were less dramatic than that of the AuNR case above.

To pinpoint the location of SERS response, control experiments were carried out. Dimethylamine (**2**) and

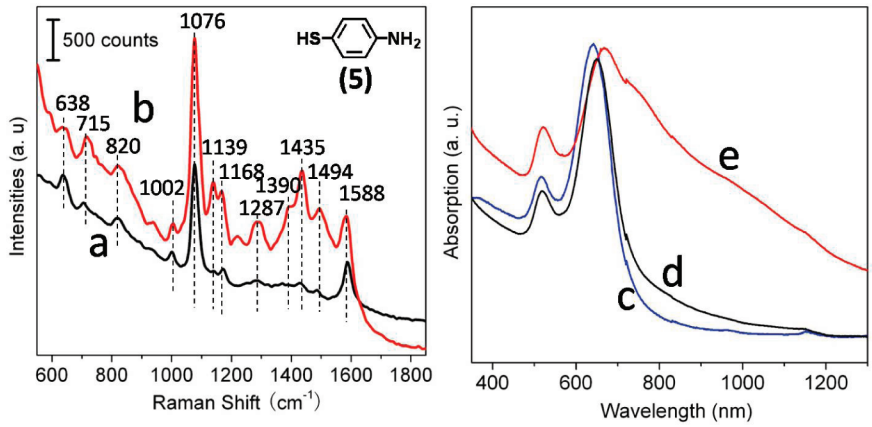

Figure 4. SERS spectra of 5-functionalized AuNRs (a) and their aggregates (b); and UV−vis−NIR absorption of as-synthesized AuNRs (c), 5-AuNRs (d), and aggregates of 5-AuNRs (induced by addition of NaCl) (e) .

3 were used as competing ligands to prepare *aniso*-(**2**+**3**-AuNR)@PSPAA. Both **2** and **3** are virtually SERS-inactive, and **2** is a weaker ligand than **1**. Thus, the NRs could be linearly assembled (similar to Figure 1m and Figure 2b, see Supporting Information) with no obvious SERS peaks (Figure 1j). After the aggregates were purified and redispersed in water, the sample was incubated with excess **1** to replace **2**. The appearance of the SERS peaks of **1** (Figure 1k) thus indicated successful ligand exchange in the preformed linear chains. Specifically, **2** should attach to the unencapsulated areas at/between the ends of AuNRs. However, the spectrum resembled that of nonaggregated *aniso*-(**1**+**3**-AuNR)@PSPAA and did not show noticeable intensity at 715, 998, and 1124 cm^{-1} (Figure 1k). Hence, it is clear that the analytes at the exchangeable positions do not contribute to the new peaks. Considering the curved ends of AuNRs, there should exist some exchangeable positions near (but not inside) the contact point. Analytes at such positions are expected to be significantly enhanced.[4,22,23,26] The molecules trapped inside the contact area should not be exchangeable as it would require considerable energy to overcome the physical stress, and on the other hand, the preexisting hotspots would unlikely exert any stress on the incoming ligands at the exchangeable positions outside the contact area. Therefore, this control experiment provides additional support that the new spectral features of Figure 1i arose from the contact points between the AuNRs. The dramatic transformation of the SERS fingerprint in Figure 1i cannot be attributed to the linear chains of AuNRs, but should be attributed to molecular reorientation *inside* the hotspots.

We studied other analytes to explore the generality of this phenomenon. A SERS-active ligand, 5,6-dimethyl-1,10-phenanthroline (**4**), is slightly soluble in water and can exchange for **2** in *aniso*-(**2**+**3**-AuNR)@PSPAA (Figure 3c),[29] possibly with an edge-on conformation on the ends of AuNRs through Au−N bonds.[41] The resulting SERS spectrum (Figure 3a) is consistent with that of **4** on nonaggregated AuNRs (see Supporting Information). After the salt-induced linear aggregation (Figure 3d), significant spectral changes were observed (Figure 3b). Similar to the previous cases, the enhancement was not equal for all peaks. Specifically, new peaks appeared at 933 and 1071 cm^{-1}, and the peaks at 650, 1145, 1280, and 1439 cm^{-1} were significantly enhanced. In contrast, the peak at 841 cm^{-1} barely changed. Since **4** is not a common SERS analyte, the exact peak assignment is not available in the literature. Nevertheless, the significant change in the SERS fingerprint was likely due to the reorientation of **4** under stress in hotspots.

In addition, 4-aminothiolphenol (**5**) was employed as analyte for its similar molecular structure as that of **1**. As-synthesized AuNRs[42] (aspect ratio of ~2.5, length = 55.6 ± 2.6 nm, and diameter = 22.3 ± 3.4 nm) were purified to remove the excess hexadecyltrimethylammonium bromide (CTAB) and then used directly as SERS enhancer, as we were not able to incorporate the positively charged **5** in partially encapsulated AuNR@PSPAA nanoparticles. After incubation of the purified AuNRs with **5** (**5**-AuNRs), the resulting SERS spectrum (Figure 4a) showed characteristic peaks of **5** in nearly upright conformation[43,44] indicating the successful exchange of CTAB by **5**. In the UV−vis spectrum, the plasmon absorption peaks were only slightly red-shifted (Figure 4d), suggesting absence of aggregation.

Upon NaCl addition, a broad absorption shoulder at 800−1200 nm (Figure 4e) indicated serious aggregation of the **5**-AuNRs. Although the randomly aggregated **5**-AuNRs probably did not favorably enhance the molecules trapped at the hotspots, the resulting SERS spectrum resembled that of **1**. The prominent peaks at 715, 1002, 1076, 1139, 1168, and 1588 cm^{-1} in Figure 4b have corresponding peaks in the SERS spectrum of **1** (Figure 1). While the two sets of aggregation-induced SERS features coincided, the detailed assignment of these peaks for **1**[30−32] and **5**[43−45] in the literature differ slightly, particularly regarding peaks at 1002 and 1076 cm^{-1}. Nevertheless, the assigned peaks are generally consistent with the hotspot-

induced reorientation hypothesis discussed above. Analyte **5** has both −SH and $-NH_2$ groups that could coordinate to the Au surface, rendering the molecule favorable for attaching in parallel conformation. Among the originally silent modes of **5** that turned into strong peaks after the aggregation, the peaks at 1139, 1390, and 1435 cm^{-1} were assigned as b_2 modes of **5**.[43] The specific enhancement of the b_2 modes was previously observed when **5** was incorporated in AgNS-**5**-AuNR sandwich nanostructures (compared to the SERS of **5**-AuNR), and it was attributed to charge transfer between metal and **5** (chemical enhancement).[45] The difference between the AgNS-**5**-AuNR and **5**-AuNR is likely the hotspot-induced orientation change of the analyte molecules. The peaks at 638 and 1588 cm^{-1} were assigned as in-plane modes of **5**;[44] they remained nearly unchanged after the aggregation. This is consistent with molecular reorientation of **5** from nearly upright to tilted/parallel conformation.

SUMMARY

The ensemble-averaged characterization of colloidal nanostructures avoids the problems associated with SERS "blinking" and minimizes photodamage of analytes. In our system, the synthesis of structurally well-defined colloidal hotspots allows the localization of SERS analytes and the isolation of the effects from within the hotspots. In addition, the linear arrangement of AuNRs specifically magnifies the SERS response at hotspots. Under such optimized conditions, a dramatic transformation of the SERS fingerprint was unambiguously demonstrated. While this phenomenon could be less pronounced in other systems, it should be quite general considering the surface selection rule and also the generality of stress-induced orientation change of surface molecules. In this report, we provide three cases using different analytes and different hotspots to demonstrate the phenomenon. In the literature, there was at least one reported case where a change of the SERS fingerprint was associated with salt-induced aggregation,[46] although it was only briefly mentioned without detailed study.

However, it should be noted that not all SERS analytes showed significant change in fingerprint upon hotspots formation. For example, a hydrophobic ligand 2-naphathlenethiol in the hotspots of silver nanospheres did not show such a phenomenon.[47]

To employ hotspots for ultrasensitive SERS detection, understanding the variability of SERS response is of great significance. Without such knowledge, SERS fingerprints could be misinterpreted and the enhancement factor at hotspots could be wrongly estimated. For example, the enhancement factor based on the 998 cm^{-1} peak in Figure 1 would be wrong if we did not account for the population change of upright *versus* tilted molecules. The correlation of SERS response with molecular orientation is of fundamental significance; further studies are imperative to fully understand the underlying mechanisms and theories. Our unique system allows us to attribute the transformation of SERS fingerprint specifically to the formation of hotspots; it also provides a platform to further explore SERS responses from hotspots.

MATERIALS AND METHODS

Materials. All chemical reagents were used without further purification. 4-Mercaptobenzoic acid 90% (tech) (**1**) and hexadecyltrimethylammonium bromide (CTAB) were purchased from Sigma Aldrich; 2-dipalmitoyl-*sn*-glycero-3-phosphothioethanol (sodium salt) (**3**) was purchased from Avanti Polar Lipids; dimethylamine (**2**), 5,6-dimethyl-1,10-phenanthroline (**4**), 4-aminothiolphenol (**5**), 2-phenyl-1-ethanethiol, sodium citrate dihydrate, and hydrogen tetrachloroaurate (III) hydrate 99.9% (metal basis Au 49%) were purchased from Alfa Aesar; amphiphilic diblock copolymers polystyrene-*block*-poly(acrylic acid) PS_{144}-*b*-PAA_{28}, M_n = 15000 for the PS block and M_n = 1600 for the PAA block, M_w/M_n = 1.11 and polystyrene-*block*-poly(acrylic acid) PS_{154}-*b*-PAA_{60}, M_n = 16000 for the PS block and M_n = 4300 for the PAA block, M_w/M_n = 1.15 were purchased from Polymer Source Inc.; 200 mesh copper specimen grids with Formvar/carbon support film (referred to as TEM grids in text) were purchased from Electron Microscopy Sciences. Ultrapure water with resistivity >18 $M\Omega \cdot cm^{-1}$ was used for all experiments.

Charaterization. TEM images were collected from JEM-1400 transmission electron microscopy operated at 120 kV. All Raman spectra were collected from colloidal nanoparticle samples in a cuvette (path length = 1.00 cm) on an R-3000HR spectrometer (Raman Systems, Inc., R-3000 series) using red LED laser (λ = 785 nm); acquisition times are 30 s for all spectra. UV−vis−NIR absorptions were carried out using a UV-3600 SHIMADZU UV−vis−NIR spectrometer.

Preparation of TEM Sample. $(NH_4)_6Mo_7O_{24} \cdot 4H_2O$ (3.4 mM in H_2O) was used as stain to enhance the contrast of polymer in all TEM images; the polymeric micelles appear white against the stained background. To improve the hydrophilicity, TEM grids were exposed in oxygen plasma for 1 min in a Harrick plasma cleaner/sterilizer. TEM grid was then placed in contact with the stained solution through the hydrophilic face. The excess solution on the TEM grid was wicked off by a filter paper, followed by drying in air for 5 min.

Synthesis and Encapsulation. AuNSs of 98 and 60 nm[48] and AuNRs[42] (aspect ratio of ~2.5, length 55.6 ± 2.6 nm, and diameter 22.3 ± 3.4 nm) were prepared by modified syntheses following the literature reports. The methods for polymer encapsulations were based on our previous reports with some modifications.[27,28,37,49,50]

Preparation of 1-AuNSs. A 1.5 mL portion of citrate-stabilized AuNSs (98 nm) was concentrated to 10 μL by centrifugation at 2900*g* for 10 min, and then incubated in 1.1 mL solution of **1** (20 mM) and NaOH (3 M). After 8 h, the sample was used for Raman characterization (Figure 1a). The same sample was then incubated at 60 °C for 3 h (Figure 1b). The large AuNSs were in low concentration (1.33×10^{-11} M) and not prone to aggregation. Finally, 10 μL of aq NaCl (5 M) was added to this sample at room temperature to induce aggregation. SERS characterization was carried out after 2 h (Figure 1c).

Synthesis of *aniso*-(1+3-AuNR)@PSPAA. The *aniso*-(**1**+**3**-AuNR)@PSPAA were synthesized by the self-assembly of PS_{144}-*b*-PAA_{28} on AuNRs in the presence of **1** and **3**.[27] In detail, the as-synthesized AuNRs (1.5 mL) was concentrated by centrifugation at 8100*g* for 10 min, and the supernatant was removed. The concentrated AuNRs solution (about 15 μL) was diluted with water

to 1.5 mL and centrifuged again to further remove the excess CTAB. The deep green solution (15 μL) collected was then diluted to 250 μL by water. A 750 μL DMF solution was prepared by mixing PS_{144}-*b*-PAA_{28} (80 μL, 8 mg/mL in DMF) with DMF (670 μL), followed by the addition of **1** (20 μL, 2 mM in ethanol). After mixing this solution with the AuNRs solution, ligand **3** (40 μL, 2 mg/mL in EtOH) was finally added. The mixture was heated at 110 °C for 2 h and then gradually cooled in an oil bath until room temperature. After that, two tubes of 200 μL as-synthesized *aniso*-(**1**+**3**-AuNR)@PSPAA were diluted to 1500 μL with water, respectively, concentrated to about 8 μL by centrifugation at 8100*g* for 10 min, and combined together. The combined *aniso*-(**1**+**3**-AuNR)@PSPAA was redispersed in 1.1 mL of DI water for the SERS characterization (Figure 1h). To prepare the linear aggregates, two tubes of 200 μL of as-synthesized *aniso*-(**1**+**3**-AuNR)@PSPAA were concentrated by centrifugation (8 μL each) and combined, followed by incubating overnight with 5 μL of NaOH (10 mM) and 5 μL of NaCl (1 M). Then, the sample was diluted to 1.5 mL, centrifuged to remove the supernatant, and redispersed in 1.1 mL of water for further characterization (Figure 1i,m). The *aniso*-(**2**+**3**-AuNR)@PSPAA particles were synthesized and linearly aggregated using the same method (see Supporting Information for details). After the purification of *aniso*-(**2**+**3**-AuNR)@PSPAA linear chains in water, they were incubated with **1** (0.036 mM in H_2O) in 1.1 mL of basic solution (0.1 mM NaOH) at 60 °C for 24 h. The sample was concentrated by centrifugation to remove the supernatant and then redispersed in 1.1 mL of water for SERS characterization (Figure 1k).

Ligand Exchange of 2 by 4 in *aniso*-(2+3-AuNR)@PSPAA. The ligand exchange of *aniso*-(**2**+**3**-AuNR)@PSPAA was carried out by incubating them with **4** and NaOH (0.714 mM) at room temperature. After 24 h, the sample was purified to remove the supernatant and then redispersed in 1.1 mL of water for SERS characterization (Figure 3a). This sample was concentrated by centrifugation (to about 40 μL) and incubated with 10 μL of NaOH (10 mM) and 10 μL of NaCl (1 M). The resulting linear aggregates were purified to remove the supernatant and redispersed in 1.1 mL of water for SERS characterization (Figure 3b).

Preparation of 5-AuNRs and Their Aggregates. A 1.5 mL portion of AuNRs was repeatedly purified to remove the large excess of CTAB as demonstrated above. The isolated AuNRs were topped up to 1 mL, and then ligand **5** (10 μL, 10 mM in ethanol) was added. After 3 h incubation, the solution was used for Raman and UV-vis-NIR absorption characterization. Aggregation of **5**-AuNRs was induced by adding 35 μL of NaCl (2.5 M). Further characterizations were carried out after 10 min reaction.

Acknowledgment. The authors thank the Ministry of Education, Singapore (ARC 27/07 and 13/09), for financial support.

Supporting Information Available: Detailed experimental procedures, large views of TEM images, and some UV−vis−NIR absorption spectra and SERS spectra. This material is available free of charge *via* the Internet at http://pubs.acs.org.

REFERENCES AND NOTES

1. Mulvihill, M.; Tao, A.; Benjauthrit, K.; Arnold, J.; Yang, P. D. Surface-Enhanced Raman Spectroscopy for Trace Arsenic Detection in Contaminated Water. *Angew. Chem., Int. Ed.* **2008**, *47*, 6456–6460.
2. Rosi, N. L.; Mirkin, C. A. Nanostructures in Biodiagnostics. *Chem. Rev.* **2005**, *105*, 1547–1562.
3. Nie, S. M.; Emery, S. R. Probing Single Molecules and Single Nanoparticles by Surface-Enhanced Raman Scattering. *Science* **1997**, *275*, 1102–1106.
4. Camargo, P. H. C.; Rycenga, M.; Au, L.; Xia, Y. N. Isolating and Probing the Hot Spot Formed between Two Silver Nanocubes. *Angew. Chem., Int. Ed.* **2009**, *48*, 2180–2184.
5. Ko, H.; Singamaneni, S.; Tsukruk, V. V. Nanostructured Surfaces and Assemblies as SERS Media. *Small* **2008**, *4*, 1576–1599.
6. Doering, W. E.; Piotti, M. E.; Natan, M. J.; Freeman, R. G. SERS as a Foundation for Nanoscale, Optically Detected Biological Labels. *Adv. Mater.* **2007**, *19*, 3100–3108.
7. Le Ru, E. C.; Meyer, M.; Blackie, E.; Etchegoin, P. G. Advanced Aspects of Electromagnetic SERS Enhancement Factors at a Hot Spot. *J. Raman Spectrosc.* **2008**, *39*, 1127–1134.
8. Moskovits, M.; DiLella, D. P. Surface-Enhanced Raman Spectroscopy of Benzene and Benzene-d_6 Adsorbed on Silver. *J. Chem. Phys.* **1980**, *73*, 6068–6075.
9. Otto, A. The 'Chemical' (Electronic) Contribution to Surface-Enhanced Raman Scattering. *J. Raman Spectrosc.* **2005**, *36*, 497–509.
10. Bolboaca, M.; Iliescu, T.; Paizs, C.; Irimie, F. D.; Kiefer, W. Raman, Infrared, and Surface-Enhanced Raman Spectroscopy in Combination with *ab Initio* and Density Functional Theory Calculations on 10-Isopropyl-10*H*-phenothiazine-5-oxide. *J. Phys. Chem. A* **2003**, *107*, 1811–1818.
11. Cui, L.; Liu, Z.; Duan, S.; Wu, D. Y.; Ren, B.; Tian, Z. Q.; Zou, S. Z. Orientation Change of Adsorbed Pyrazine on Roughened Rhodium Electrodes as Probed by Surface-Enhanced Raman Spectroscopy. *J. Phys. Chem. B* **2005**, *109*, 17597–17602.
12. Moskovits, M.; Suh, J. S. Surface Geometry Change in 2-Naphthoic Acid Adsorbed on Silver. *J. Phys. Chem.* **1988**, *92*, 6327–6329.
13. Barhoumi, A.; Zhang, D. M.; Halas, N. J. Correlation of Molecular Orientation and Packing Density in a dsDNA Self-Assembled Monolayer Observable with Surface-Enhanced-Raman Spectroscopy. *J. Am. Chem. Soc.* **2008**, *130*, 14040–14041.
14. Shegai, T. O.; Haran, G. Probing the Raman Scattering Tensors of Individual Molecules. *J. Phys. Chem. B* **2006**, *110*, 2459–2461.
15. Brus, L. Noble Metal Nanocrystals: Plasmon Electron Transfer Photochemistry and Single-Molecule Raman Spectroscopy. *Acc. Chem. Res.* **2008**, *41*, 1742–1749.
16. Qian, X. M.; Nie, S. M. Single-Molecule and Single-Nanoparticle SERS: From Fundamental Mechanisms to Biomedical Applications. *Chem. Soc. Rev.* **2008**, *37*, 912–920.
17. Fang, Y.; Seong, N.-H.; Dlott, D. D. Measurement of the Distribution of Site Enhancements in Surface-Enhanced Raman Scattering. *Science* **2008**, *321*, 388–392.
18. Camden, J. P.; Dieringer, J. A.; Wang, Y. M.; Masiello, D. J.; Marks, L. D.; Schatz, G. C.; Van Duyne, R. P. Probing the Structure of Single-Molecule Surface-Enhanced Raman Scattering Hot Spots. *J. Am. Chem. Soc.* **2008**, *130*, 12616–12617.
19. Braun, G.; Pavel, I.; Morrill, A. R.; Seferos, D. S.; Bazan, G. C.; Reich, N. O.; Moskovits, M. Chemically Patterned Microspheres for Controlled Nanoparticle Assembly in the Construction of SERS Hot Spots. *J. Am. Chem. Soc.* **2007**, *129*, 7760–7761.
20. Braun, G. B.; Lee, S. J.; Laurence, T.; Fera, N.; Fabris, L.; Bazan, G. C.; Moskovits, M.; Reich, N. O. Generalized Approach to SERS-Active Nanomaterials *via* Controlled Nanoparticle Linking, Polymer Encapsulation, and Small-Molecule Infusion. *J. Phys. Chem. C* **2009**, *113*, 13622–13629.
21. Lassiter, J. B.; Aizpurua, J.; Hernandez, L. I.; Brandl, D. W.; Romero, I.; Lal, S.; Hafner, J. H.; Nordlander, P.; Halas, N. J. Close Encounters Between Two Nanoshells. *Nano Lett.* **2008**, *8*, 1212–1218.
22. Li, W. Y.; Camargo, P. H. C.; Lu, X. M.; Xia, Y. N. Dimers of Silver Nanospheres: Facile Synthesis and Their Use as Hot Spots for Surface-Enhanced Raman Scattering. *Nano Lett.* **2009**, *9*, 485–490.
23. Li, W. Y.; Camargo, P. H. C.; Au, L.; Zhang, Q.; Rycenga, M.; Xia, Y. N. Etching and Dimerization: A Simple and Versatile Route to Dimers of Silver Nanospheres with a Range of Sizes. *Angew. Chem., Int. Ed.* **2010**, *49*, 164–168.
24. Chen, G.; Wang, Y.; Tan, L. H.; Yang, M. X.; Tan, L. S.; Chen, Y.; Chen, H. Y. High-Purity Separation of Gold Nanoparticle Dimers and Trimers. *J. Am. Chem. Soc.* **2009**, *131*, 4218–4219.
25. Dadosh, T.; Sperling, J.; Bryant, G. W.; Breslow, R.; Shegai,

T.; Dyshel, M.; Haran, G.; Bar-Joseph, I. Plasmonic Control of the Shape of the Raman Spectrum of a Single Molecule in a Silver Nanoparticle Dimer. *ACS Nano* **2009**, *3*, 1988–1994.
26. Hui, W.; Kundu, J.; Halas, N. J. Plasmonic Nanoshell Arrays Combine Surface-Enhanced Vibrational Spectroscopies on a Single Substrate. *Angew. Chem., Int. Ed.* **2007**, *46*, 9040–9044.
27. Tan, L. H.; Xing, S. X.; Chen, T.; Chen, G.; Huang, X.; Zhang, H.; Chen, H. Y. Fabrication of Polymer Nanocavities with Tailored Openings. *ACS Nano* **2009**, *3*, 3469–3474.
28. Yang, M. X.; Chen, T.; Lau, W. S.; Wang, Y.; Tang, Q. H.; Yang, Y. H.; Chen, H. Y. Development of Polymer-Encapsulated Metal Nanoparticles as Surface-Enhanced Raman Scattering Probes. *Small* **2009**, *5*, 198–202.
29. Feng, Y. H.; Xing, S. X.; Xu, J.; Wang, H.; Lim, J. W.; Chen, H. Y. Probing the Kinetics of Ligand Exchange on Colloidal Gold Nanoparticles by Surface-Enhanced Raman Scattering. *Dalton Trans.* **2010**, *39*, 349–351.
30. Bishnoi, S. W.; Rozell, C. J.; Levin, C. S.; Gheith, M. K.; Johnson, B. R.; Johnson, D. H.; Halas, N. J. All-Optical Nanoscale pH Meter. *Nano Lett.* **2006**, *6*, 1687–1692.
31. Michota, A.; Bukowska, J. Surface-Enhanced Raman Scattering (SERS) of 4-Mercaptobenzoic Acid on Silver and Gold Substrates. *J. Raman Spectrosc.* **2003**, *34*, 21–25.
32. Orendorff, C. J.; Gole, A.; Sau, T. K.; Murphy, C. J. Surface-Enhanced Raman Spectroscopy of Self-Assembled Monolayers: Sandwich Architecture and Nanoparticle Shape Dependence. *Anal. Chem.* **2005**, *77*, 3261–3266.
33. Park, H.; Lee, S. B.; Kim, K.; Kim, M. S. Surface-Enhanced Raman Scattering of *p*-Aminobenzoic Acid at Silver Electrode. *J. Phys. Chem.* **1990**, *94*, 7576–7580.
34. Cho, S. H.; Han, H. S.; Jang, D.-J.; Kim, K.; Kim, M. S. Raman Spectroscopic Study of 1,4-Benzenedithiol Adsorbed on Silver. *J. Phys. Chem.* **1995**, *99*, 10594–10599.
35. Rycenga, M.; Kim, M. H.; Camargo, P. H. C.; Cobley, C.; Li, Z. Y.; Xia, Y. N. Surface-Enhanced Raman Scattering: Comparison of Three Different Molecules on Single-Crystal Nanocubes and Nanospheres of Silver. *J. Phys. Chem. A* **2009**, *113*, 3932–3939.
36. Love, J. C.; Estroff, L. A.; Kriebel, J. K.; Nuzzo, R. G.; Whitesides, G. M. Self-Assembled Monolayers of Thiolates on Metals as a Form of Nanotechnology. *Chem. Rev.* **2005**, *105*, 1103–1169.
37. Chen, T.; Yang, M. X.; Wang, X. J.; Tan, L. H.; Chen, H. Y. Controlled Assembly of Eccentrically Encapsulated Gold Nanoparticles. *J. Am. Chem. Soc.* **2008**, *130*, 11858–11859.
38. Xu, H. X. Calculation of the near Field of Aggregates of Arbitrary Spheres. *J. Opt. Soc. Am. A* **2004**, *21*, 804–809.
39. Moskovits, M.; Suh, J. S. Conformaiton of Mono- and Dicarboxylic Acids Adsorbed on Silver Surfaces. *J. Am. Chem. Soc.* **1985**, *107*, 6826–6829.
40. Wu, D.; Fang, Y. The Adsorption Behavior of *p*-Hydroxybenzoic Acid on a Silver-Coated Filter Paper by Surface Enhanced Raman Scattering. *J. Colloid Interface Sci.* **2003**, *265*, 234–238.
41. Muniz-Miranda, M. Surface Enhanced Raman Scattering and Normal Coordinate Analysis of 1,10-Phenanthroline Adsorbed on Silver Sols. *J. Phys. Chem. A* **2000**, *104*, 7803–7810.
42. Gole, A.; Murphy, C. J. Azide-Derivatized Gold Nanorods: Functional Materials for "Click" Chemistry. *Langmuir* **2008**, *24*, 266–272.
43. Zheng, J. W.; Li, X. W.; Gu, R. N.; Lu, T. H. Comparison of the Surface Properties of the Assembled Silver Nanoparticle Electrode and Roughened Silver Electrode. *J. Phys. Chem. B* **2002**, *106*, 1019–1023.
44. Osawa, M.; Matsuda, N.; Yoshii, K.; Uchida, I. Charge Transfer Resonance Raman Process in Surface-Enhanced Raman Scattering from *p*-Aminothiophenol Adsorbed on Silver: Herzberg–Teller Contribution. *J. Phys. Chem.* **1994**, *98*, 12702–12707.
45. Hu, X. G.; Wang, T.; Wang, L.; Dong, S. J. Surface-Enhanced Raman Scattering of 4-Aminothiophenol Self-Assembled Monolayers in Sandwich Structure with Nanoparticle Shape Dependence: Off-Surface Plasmon Resonance Condition. *J. Phys. Chem. C* **2007**, *111*, 6962–6969.
46. Su, X.; Zhang, J.; Sun, L.; Koo, T. W.; Chan, S.; Sundararajan, N.; Yamakawa, M.; Berlin, A. A. Composite Organic–Inorganic Nanoparticles (COINs) with Chemically Encoded Optical Signatures. *Nano Lett.* **2005**, *5*, 49–54.
47. Chen, G.; Wang, Y.; Yang, M.; Xu, J.; Goh, S. J.; Pan, M.; Chen, H. Measuring Ensemble-Averaged Surface-Enhanced Raman Scattering in the Hotspots of Colloidal Nanoparticle Dimers and Trimers. *J. Am. Chem. Soc.* **2010**, *132*, 3644–3645.
48. Frens, G. Controlled Nucleation for the Regulation of the Particle Size in Monodispersed Colloidal Gold Suspension. *Nat. Phys. Sci.* **1973**, *241*, 20–22.
49. Chen, H. Y.; Abraham, S.; Mendenhall, J.; Delamarre, S. C.; Smith, K.; Kim, I.; Batt, C. A. Encapsulation of Single Small Gold Nanoparticles by Diblock Copolymers. *Chemphyschem* **2008**, *9*, 388–392.
50. Wang, X. J.; Li, G. P.; Chen, T.; Yang, M. X.; Zhang, Z.; Wu, T.; Chen, H. Y. Polymer-Encapsulated Gold-Nanoparticle Dimers: Facile Preparation and Catalytical Application in Guided Growth of Dimeric ZnO-Nanowires. *Nano Lett.* **2008**, *8*, 2643–2647.